NUCL SCI TECH (2022) 33:55
https://doi.org/10.1007/s41365-022-01048-4

Production of p-rich nuclei with $Z = 20 - 25$ based on radioactive ion beams

Bing Li[1,2] · Na Tang[1,2] · Yu-Hai Zhang[1,2] · Feng-Shou Zhang[1,2,3]

Received: 22 February 2022 / Revised: 27 March 2022 / Accepted: 1 April 2022 / Published online: 15 June 2022

Abstract Within the framework of isospin-dependent Boltzmann-Langevin model, the production cross sections of proton-rich nuclei with $Z = 20 - 25$ are investigated. According to the reaction results for different isospin of projectiles ^{48}Ni, ^{49}Ni, and ^{50}Ni, proton-rich fragments tend to be more easily produced in reactions with the proton-rich projectile ^{48}Ni. The production cross sections of the unknown nuclei in the vicinity of the projectile are sensitive to incident energy. It is observed that incident energy of 345 MeV/u is appropriate for producing proton-rich nuclei with $Z = 20 - 25$. In projectile fragmentation reactions based on the radioactive ion beam of ^{48}Ni at 345 MeV/u, several unknown proton-rich nuclei near the proton drip line are generated in the simulations. All these new nuclei are near-projectile elements near $Z = 28$. The production cross sections of the new nuclei ^{34}Ca, ^{37,38}Sc, ^{38}Ti, ^{40,41,42}V, ^{40,41}Cr, and ^{42,43,44,45}Mn are in the range of 10^{-2}–10^{2} mb. Hence, projectile fragmentation of radioactive ion beams of Ni is a potential method for generating new proton-rich nuclei with $Z = 20 - 25$.

This work was Supported by the National Natural Science Foundation of China (No. 12135004, No. 11635003 and No. 11961141004).

✉ Feng-Shou Zhang
fszhang@bnu.edu.cn

[1] Key Laboratory of Beam Technology of the Ministry of Education, College of Nuclear Science and Technology, Beijing Normal University, Beijing 100875, China

[2] Institute of Radiation Technology, Beijing Academy of Science and Technology, Beijing 100875, China

[3] Center of Theoretical Nuclear Physics, National Laboratory of Heavy Ion Accelerator of Lanzhou, Lanzhou 730000, China

Keywords Production cross sections · Radioactive ion beams · Isospin-dependent Boltzmann-Langevin model

1 Introduction

The production of new exotic isotopes and determination of drip lines are frontier topics in nuclear physics [1–6]. To date, 3327 nuclides have been experimentally observed [7]. Erler et al. predicted the presence of approximately 7000 nuclides; therefore, more than half of these nuclides remain undiscovered [1, 8]. Investigation of exotic isotopes provides valuable information for understanding the processes of nuclear astrophysics and nuclear structure [9–12]. Moreover, this types of nuclear reactions provide further information on isospin dependent nucleon–nucleon interactions, offering a powerful method to study the nuclear equation of state and even the symmetry energy, which is important for the physics of neutron stars and supernovas [13–18].

To date, the proton drip line experimentally reached the medium-mass region, whereas the neutron drip line has only recently been detected up to $Z = 10$ [8, 19, 20]. The proton drip line is closer to the stable region because of the Coulomb repulsion between protons, which leads to a long lifetime even for nuclides outside the proton drip line [21]. This results in shallow regions or sandbanks, which serve to bridge gaps of unbound nuclei along the path of the astrophysical rapid-proton capture (*rp*) process [22]. Additionally, approximately 200 proton unbound nuclides remain to be discovered [8]. Some of these nuclides are reconstructed through their decay products, and some even have lifetimes long enough to be experimentally observable. With the establishment of sophisticated facilities,

radioactive ion beams (RIBs) of nuclei with large excesses of neutrons or protons allow a deeper investigation of exotic isotopes, which has led to new discoveries such as halo nuclei and the change of magic numbers with isospin [23–26]. The separation and identification of exotic nuclei have become principally possible using two techniques: isotope separation online (ISOL) and in-flight separation techniques [27–32]. In particular, the cross sections of intermediate mass fragments under projectile fragmentation reactions at 140 MeV/u were investigated at the National Superconducting Cyclotron Laboratory (NSCL) at Michigan State University (MSU) using an A1900 fragment separator [4]. Recently, the proton-rich isotope ^{68}Br was discovered in secondary fragmentation reactions at the RIKEN Nishina Center in 2019, suggesting that secondary fragmentation reactions offer an alternative way to search for new isotopes [21]. Similar experimental and theoretical studies have been conducted [33–39].

Exotic nuclei can be generated via projectile fragmentation, fission, and spallation [2, 40, 41]. Spallation is an effective reaction mechanism for the production of exotic nuclei for time-of-flight particle identification [42–44]. High-energy projectile fission is appropriate for light and heavy fission fragments [45–47]. Projectile fragmentation is a common reaction mechanism that has recently been used to study the production of new exotic nuclei, and many new nuclides have been discovered [48–52]. Recently, multinucleon transfer in peripheral reactions at beam energies from the Coulomb barrier to the Fermi energy has been considered to exhibit the potential of producing exotic nuclei because the projectile can pick up neutrons from the neutron-rich target [53–57].

The development of projectile fragmentation for producing new radioactive nuclides has led to a new era, not only in the discovery of new nuclides, but also in the generation and utilization of unstable RIBs. Models describing projectile fragmentation reactions deliver important inputs for yield predictions that are useful for planning experiments and future accelerator facilities [58]. The models include Boltzmann-Uehling-Uhlenbeck (BUU) model [59–61], quantum molecular dynamics (QMD) model [62–66], the stochastic mean-field approach (SMF) [14, 67, 68], the abrasion–ablation (AA) model [69–71], the empirical parameterization of fragmentation cross sections (EPAX) [72–74], and the FRACS parameterization [75–77]. Transport models are good event generators and exhibit applications, for example, to design or simulate new detectors, and empirical approaches also provide better agreement with the experimental data within a large range of incident energy [78, 79]. For a thorough review, refer to Refs. [80–85]. The theoretical method applied in this study was developed by adding the fluctuating collision term to the BUU equation and introducing the isospin effect, which is the isospin-dependent Boltzmann-Langevin equation (IBLE) [86–95].

In this study, we investigate the production cross sections of nuclei near the proton drip line with charge number $Z = 20 - 25$ by using RIBs in an isospin-dependent Boltzmann-Langevin approach. A good description of the experimental data with the IBLE model suggests the possibility of using the present theoretical framework for the prediction of exotic nuclei using RIBs, which will soon be available in upcoming facilities [8, 21, 35, 54]. The remainder of this paper is organized as follows. A brief introduction to the IBLE model is provided in Sect. 2. The model test, calculation results, and discussion are presented in Sect. 3. Finally, the conclusions of the study are presented in Sect. 4.

2 Theoretical descriptions

In the IBLE model, the transport equation of motion for fluctuating single-particle density $\hat{f}(\boldsymbol{r},\boldsymbol{p},t)$ can be expressed in the following form [87–89, 93]:

$$\left(\frac{\partial}{\partial t}+\frac{\boldsymbol{p}}{m}\cdot\bigtriangledown_r-\bigtriangledown_r U(\hat{f})\cdot\bigtriangledown_p\right)\hat{f}(\boldsymbol{r},\boldsymbol{p},t) = K(\hat{f})+\delta K(\boldsymbol{r},\boldsymbol{p},t), \tag{1}$$

where the left side expresses the Vlasov propagation of the individual particles in the nuclear mean field $U(\hat{f})$, while the right side describes the residual binary collisions. $K(\hat{f})$ denotes the collision term that has the usual BUU form but a stochastic character manifested by the fluctuating density $\hat{f}(\boldsymbol{r},\boldsymbol{p},t)$:

$$K(\hat{f}_1) = \int d\boldsymbol{p}_2 d\boldsymbol{p}_3 d\boldsymbol{p}_4 W(12;34) [\hat{f}_3\hat{f}_4(1-\hat{f}_1)(1-\hat{f}_2)-\hat{f}_1\hat{f}_2(1-\hat{f}_3)(1-\hat{f}_4)]. \tag{2}$$

Here, the $\hat{f}_i = \hat{f}(\boldsymbol{r}_i,\boldsymbol{p}_i,t)$ denotes the diagonal elements of single particle density and $W(12; 34)$ denotes the transition rate, which is related to the cross section of the corresponding two-body scattering process. $\delta K(\boldsymbol{r},\boldsymbol{p},t)$ is the fluctuating collision term, whose second moment is characterized by a correlation function

$$\langle\delta K(\boldsymbol{r}_1,\boldsymbol{p}_1,t_1)\delta K(\boldsymbol{r}_2,\boldsymbol{p}_2,t_2)\rangle = C(\boldsymbol{r},\boldsymbol{p}_1,\boldsymbol{p}_2)\,\delta(\boldsymbol{r}_1-\boldsymbol{r}_2)\delta(t_1-t_2), \tag{3}$$

where $\langle\cdots\rangle$ presents the average over the local ensemble of BLE events, which is the local average [87–89, 93]. The fluctuating collision term acts as a stochastic force acting

on $\hat{f}$, which is consistent with the "fluctuation–dissipation theorem." The correlation function $C(\boldsymbol{p}_1,\boldsymbol{p}_2)$ is assumed as local in space and time, and it is coherent with the Markovian treatment of the Boltzmann collision term [88, 96]. In the semi-classical limit, the correlation function is determined by the local averaged single-particle density $f(\boldsymbol{r},\boldsymbol{p},t)$ as detailed in Ref. [88].

To obtain approximate solutions of the IBLE transport equation, a projection method was introduced and applied [86, 92]. The fluctuations were projected onto a set of low-order multipole moments of the momentum distribution. The zero-order multipole moment is constant along with the first multipole moment because of mass conservation and momentum conservation. The quadrupole moment of the momentum distribution exhibits a strong dissipative phenomenon, and it can describe the fluctuations very well. The propagation of fluctuations in the quadrupole moment of the momentum distribution alone does not provide a detailed description of the momentum space fluctuations. Thus, the octupole moment of the momentum distribution is also introduced, although its dissipative effect is not evident. We expect that such an approximation can provide a reasonable description of the gross properties of the dynamics of density fluctuations in heavy-ion collisions [86]. The local multipole moments of the momentum distribution are defined as follows:

$$\hat{Q}_{LM}(\boldsymbol{r},t) = \int d\boldsymbol{p} Q_{LM}(\boldsymbol{p})\hat{f}(\boldsymbol{r},\boldsymbol{p},t), \tag{4}$$

where $Q_{LM}(\boldsymbol{p})$ is the fluctuating multipole moments of order L with magnetic quantum number M in the momentum space. The fluctuations of multipole moments can be expressed by the diffusion matrix provided by [88]

$$\begin{aligned} C_{LML'M'}(\boldsymbol{r},t) &= \int d\boldsymbol{p}d\boldsymbol{p}' Q_{LM}(\boldsymbol{p})Q_{L'M'}(\boldsymbol{p}')C(\boldsymbol{p},\boldsymbol{p}') \\ &= \int d\boldsymbol{p}_1 d\boldsymbol{p}_2 d\boldsymbol{p}_3 d\boldsymbol{p}_4 \triangle Q_{LM} \triangle Q_{L'M'} \\ &\times W(12,34) f_1 f_2 (1-f_3)(1-f_4), \end{aligned} \tag{5}$$

with $\triangle Q_{LM} = Q_{LM}(\boldsymbol{p}_1) + Q_{LM}(\boldsymbol{p}_2) - Q_{LM}(\boldsymbol{p}_3) - Q_{LM}(\boldsymbol{p}_4)$. $f_1 f_2 (1-f_3)(1-f_4)$ describes the Pauli-blocking effect. The diffusion matrix $C_{LML'M'}$ can reliably describe the dynamics of multipole moments, although it contains less information on the dynamics than the correlation function $C(\boldsymbol{p},\boldsymbol{p}')$ [86].

In this model, the isospin-dependent interaction nuclear potential is provided as follows:

$$\begin{aligned} U_\tau(\rho,\delta) =& \alpha\frac{\rho}{\rho_0} + \beta\left(\frac{\rho}{\rho_0}\right)^\gamma + E_{\rm sym}^{\rm loc}(\rho)\delta^2 \\ &+ \frac{\partial E_{\rm sym}^{\rm loc}(\rho)}{\partial\rho}\rho\delta^2 + E_{\rm sym}^{\rm loc}(\rho)\rho\frac{\partial\delta^2}{\partial\rho_\tau}, \end{aligned} \tag{6}$$

where $\delta = (\rho_{\rm n} - \rho_{\rm p})/\rho$ is the isospin asymmetry; ρ_0 is normal nuclear matter density; ρ, $\rho_{\rm p}$, and $\rho_{\rm n}$ denote the total, proton, and neutron densities, respectively. We adopted the soft equation of state, which is widely applied in heavy-ion collisions at intermediate and high incident energies [88, 96]. The coefficient values of α, β, and γ are -356 MeV, 303 MeV and 7/6, respectively. $E_{\rm sym}^{\rm loc}$ is the local part of the symmetry energy, which is provided by

$$E_{\rm sym}^{\rm loc}(\rho) = \frac{1}{2}C_{\rm sym}\left(\frac{\rho}{\rho_0}\right)^{\gamma_s}, \tag{7}$$

where $\gamma_{\rm S}$ = 0.5 and 2.0 correspond to the soft and hard symmetry energies, respectively [94]. The coefficient value of $C_{\rm sym}$ was 29.4 MeV. The details on the symmetry energy are provided in Ref. [94, 95].

The cross sections of each channel used in the IBLE model are experimental parameterizations, which are isospin-dependent [97–99]. Additionally, the in-medium cross sections for each channel were used in the model as detailed in Ref. [94]. In this study, we construct clusters using the coalescence model, in which parameters R_0 and P_0 are set as 3.5 fm and 300 MeV/c, respectively [95]. Calculations were performed with 20 test particles, and simulations were conducted for 10,000 events, with impact parameter values ranging from 0 to 7 fm. The excitation energy of the produced light fragments is not sufficient to evaporate neutrons; therefore, the difference between the cross sections before and after de-excitation is small. In this study, we focus on the production cross sections of light fragments around $Z = 20$.

3 Results and discussion

To test the feasibility of using the IBLE model to predict the production cross sections of nuclei in projectile fragmentation, we calculated the cross sections of nuclei with $19 \leqslant Z \leqslant 24$ in the reaction of ^{58}Ni+^{9}Be at 140 MeV/u as shown in Fig. 1. The solid and dashed lines denote the results of the IBLE model for the hard and soft symmetry energies, respectively. The solid circles denote the experimental data obtained from Ref. [4]. As shown, the measured cross sections of the fragments are reasonably reproduced by the IBLE model for hard and soft symmetry energies. The peak locations of the calculated cross

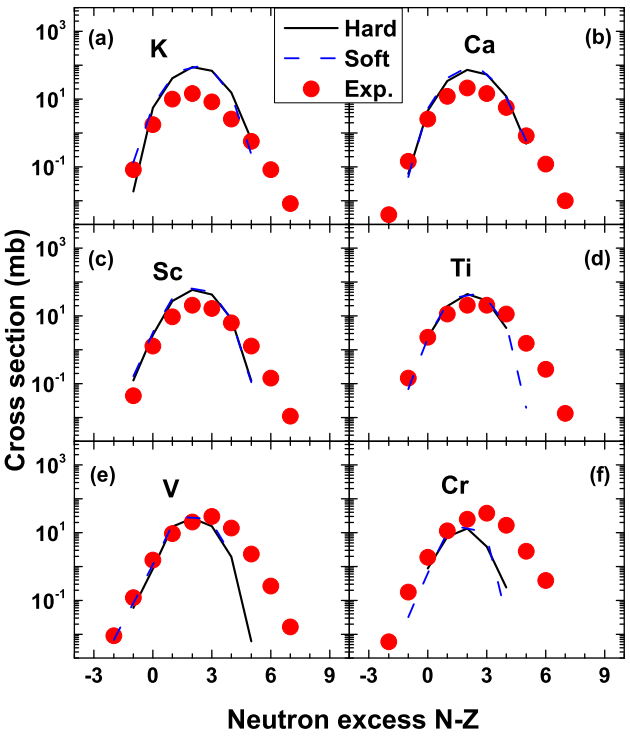

Fig. 1 (Color online) The cross sections presented as isotope distributions for $19 \leqslant Z \leqslant 24$ elements in ^{58}Ni+^{9}Be reaction at 140 MeV/u were stimulated via IBLE model for hard and soft symmetry energies and compared with the experimental data [4]

sections are close to those obtained via experiments. With respect to K and Ca, the peaks of the calculated cross sections overestimated the experimental value, and the difference was within one order of magnitude. The number of calculated isotopes is less than the experimental value, especially for fragments near the projectile, which is a limitation of dynamical simulations in IBLE, i.e., it is dependent on the number of simulated events. For the simulations of different symmetry energies, it is observed that the results are very close and differ only slightly in the proton-rich and neutron-rich regions. In the proton-rich region, more isotopes are calculated for soft symmetry energy than for hard symmetry energy. By comparing the two calculations with the experimental data, we observe that the IBLE model realizes a good description of the cross-section distributions but slightly underestimates the neutron-rich tails. The calculations for the soft symmetry energy produced more isotopes, especially for proton-rich nuclei. Therefore, it is reasonable to apply the IBLE model with soft symmetry energy to predict the production cross sections of proton-rich fragments in projectile fragmentation reactions.

Radioactive ion beams became possible with the development of large scientific installations worldwide [2, 21, 33]. To produce proton-rich nuclei with charge number $Z \approx 20$, proton-rich beams should be used in projectile fragmentation reactions. ^{48,49,50}Ni are good candidates for radioactive beams because they exhibit small N/Z ratios near $Z \approx 20$. They are most likely generated via projectile fragmentation in a newly built FRIB facility, such as the fragmentation of a ^{58}Ni beam on a beryllium target at an incident energy of several hundred MeV/u. To study the effect of isospin of the projectile on the fragments produced by projectile fragmentation, the isotopic distributions of fragments with $Z = 20 - 25$ for the ^{48}Ni+^{9}Be (circles), ^{49}Ni+^{9}Be (squares), and ^{50}Ni+^{9}Be (triangles) reactions at 140 MeV/u are shown in Fig. 2. Unknown nuclei are denoted by open symbols. The isospin T_z of projectiles ^{48}Ni, ^{49}Ni, and ^{50}Ni are -4, $-7/2$, and -3, respectively. It is observed that the produced fragments tend to be proton-rich because of proton-rich radioactive ion beams. In Fig. 2, several new nuclei near the proton drip line, such as ^{37,38}Sc, ^{38}Ti, ^{40,41,42}V, ^{41}Cr, and ^{43,44,45}Mn, are generated during simulations. The predicted production cross sections of these nuclei ranged from 10^{-2} to 10^{2} mb. The number and cross sections of proton-rich new nuclei in the reaction with ^{48}Ni projectile are the highest, which is due to the highest absolute value of the projectile isospin and the lowest N/Z ratio. As the mass

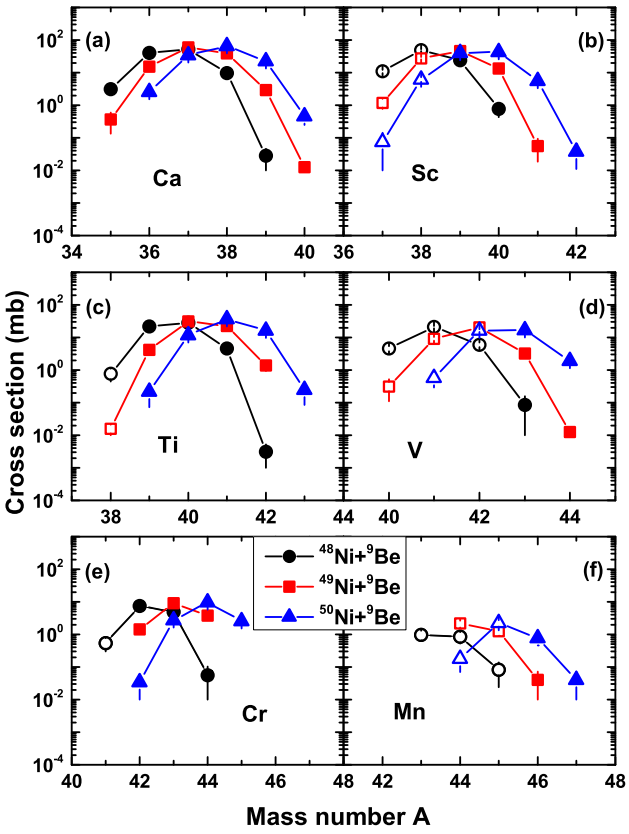

Fig. 2 (Color online) Calculated isotopic distributions of fragments with $Z = 20 - 25$ for ^{48}Ni+^{9}Be, ^{49}Ni+^{9}Be, and ^{50}Ni+^{9}Be reactions at 140 MeV/u. Unknown nuclei are denoted by the open symbols

number of the projectile increases by 1, the peak of the isotopic distribution shifts to the right by approximately one unit, which shows a strong isospin effect in the projectile fragmentation reactions because the isospin effect is dependent on the density distribution of protons and neutrons. When the absolute value of the projectile isospin decreases or when the *N*/*Z* ratio increases, the produced fragments are closer to the stability line. The absolute values of isospins of newly produced nuclei are smaller than those of the projectile because as the reaction proceeds the isospin of the reaction system gradually tends toward equilibrium, which is the isospin diffusion process.

According to the above results for different isospin of projectiles, reaction ^{48}Ni+^{9}Be exhibits the advantage of producing rare proton-rich nuclei. To observe the incident energy effect, the production cross sections of the fragments in the ^{48}Ni+^{9}Be reaction at 140 MeV/u (circles), 240 MeV/u (squares), and 345 MeV/u (triangles) are shown in Fig. 3. As shown, the production cross sections of new nuclei at 345 MeV/u are the largest, especially the nuclei near the projectile. However, the difference among the results for different incident energies is not large. The discrepancy between the fragment cross sections at the three energies increased as the charge number of the generated fragments increased. Heavy fragments are mainly produced from peripheral collisions, which vary significantly with incident energies below 200 MeV/u [4]. Additionally, the number of new nuclei produced in the simulations was consistent at incident energies of 240 and 345 MeV/u. In the ^{48}Ni+^{9}Be reaction at 140 MeV/u, the production cross sections of the produced fragments with $Z = 20$–25 decrease as charge number increases, whereas at 345 MeV/u, the production cross sections of the corresponding fragments do not show a significant decreasing trend. At 345 MeV/u, the projectile and target collide quickly with each other, resulting in fragments produced by the reaction. Furthermore, when compared to the reaction 140 MeV/u, the characteristics of the initial entrance channel are retained to the maximum extent at 345 MeV/u.

To analyze the characteristics of the fragments produced by different projectiles in projectile fragmentation reactions, the production cross sections as functions of *Z* and *A* for the fragments in the ^{48}Ni+^{9}Be (a), ^{49}Ni+^{9}Be (b), and ^{50}Ni+^{9}Be (c) reactions at 140 MeV/u are presented in Fig. 4. As the mass number of the projectile increases, the mass of the fragments produced slightly increases.

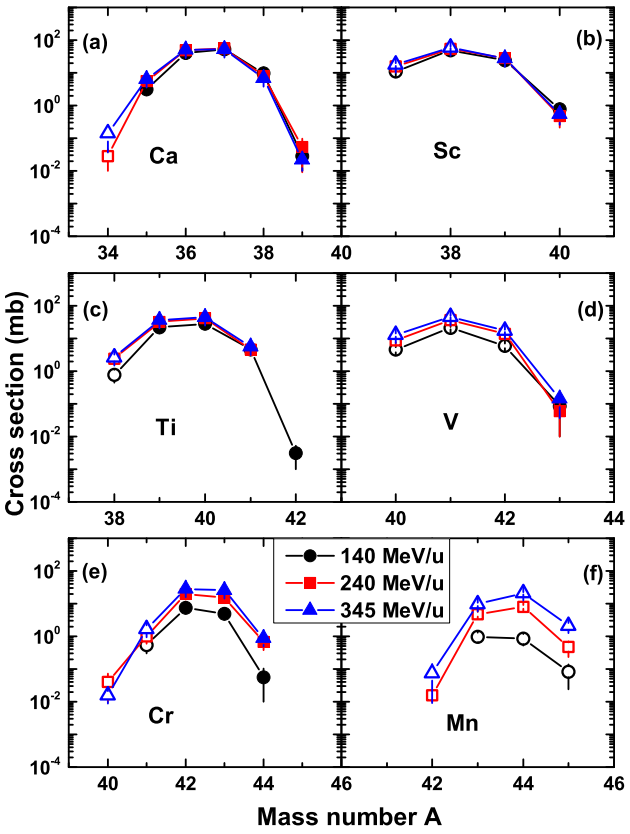

Fig. 3 (Color online) Calculated isotopic distributions of fragments with $Z = 20 - 25$ for ^{48}Ni+^{9}Be at 140, 240, and 345 MeV/u. Unknown nuclei are denoted by the open symbols

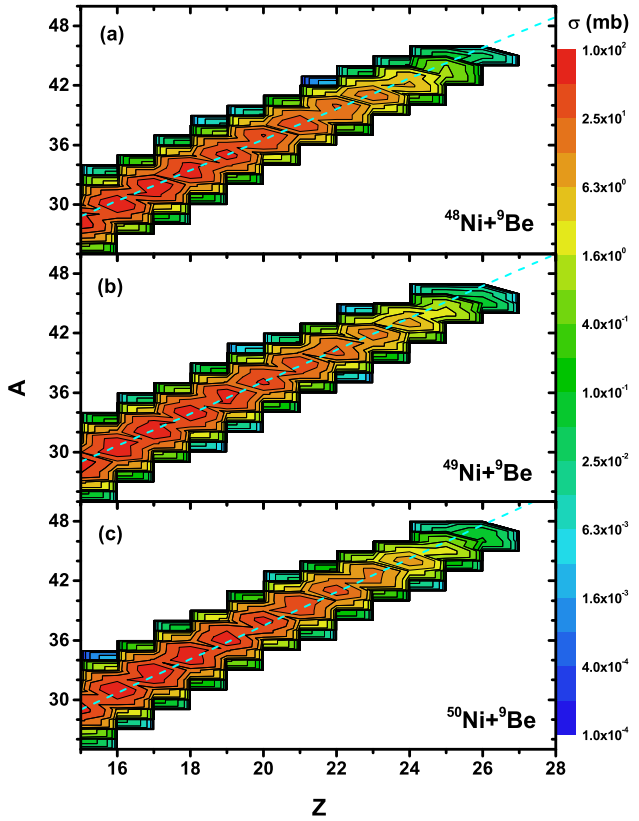

Fig. 4 (Color online) Production cross sections as functions of *Z* and *A* for the fragments in ^{48}Ni+^{9}Be, ^{49}Ni+^{9}Be, and ^{50}Ni+^{9}Be reactions at 140 MeV/u. The dashed lines indicate the general trends of the distributions

Additionally, there was a plateau near $Z = 16$ in all three reaction systems, where most of the fragments in this region were produced from the projectiles. The dashed lines indicate the general trends in the three distributions. The slopes of the dashed lines are 1.54, 1.62, and 1.69, corresponding to the reactions ^{48}Ni+^{9}Be, ^{49}Ni+^{9}Be, and ^{50}Ni+^{9}Be, respectively. An increase in the slope indicates that proton-rich fragments are difficult to produce in the reaction induced by the ^{50}Ni projectile, which is consistent with Fig. 2.

The ^{48}Ni+^{9}Be reaction at 345 MeV/u provides a significant advantage for producing new proton-rich nuclei with $Z = 20 - 25$ as discussed above. To observe the relationship between the calculated nuclei near the proton drip line and experimentally synthesized nuclei with higher intuition, a nuclear chart of the predicted fragments with $Z = 20 - 25$ for the ^{48}Ni+^{9}Be reaction at 345 MeV/u is shown in Fig. 5. The filled and open squares denote known and unknown nuclei, respectively. Black, red, and brown are stable, β^+ decay, and p decay, respectively. The production cross sections of unknown nuclei in the ^{48}Ni+^{9}Be reaction at 345 MeV/u are indicated by open squares in the figure. From the figure, it can be observed that the produced new nuclei are mainly distributed in the vicinity of the projectile (Z = 28) because the new nuclei are almost formed by the projectile sources in the region of highly peripheral collisions [30]. In the projectile fragmentation of ^{48}Ni+^{9}Be, 13 new proton-rich nuclei with $Z = 20 - 25$ have been predicted as follows: ^{34}Ca (0.14 mb), ^{37}Sc (18.2 mb), ^{38}Sc (60.3 mb), ^{38}Ti (2.61 mb), ^{40}V (12.8 mb), ^{41}V (46.5 mb), ^{42}V (17.2 mb), ^{40}Cr (15.7 μb), ^{41}Cr (1.70 mb), ^{42}Mn (75.4 μb), ^{43}Mn (9.53 mb), ^{44}Mn (21.1 mb), and ^{45}Mn (2.08 mb). Additionally, an empirical approach was applied to determine the binding energies and to predict the cross sections for isotopes with $Z = 22 - 28$ near the proton drip line (see Refs. [100, 101]). It is evident that the selection of the optimal reaction system should consider not only the production cross sections of fragments but also various factors such as experimental feasibility and detection efficiency. In any case, with the improvement of the experimental condition technology, it is expected that the generation of new proton-rich nuclei with $Z = 20 - 25$ via the ^{48,49,50}Ni+^{9}Be reaction is imminent.

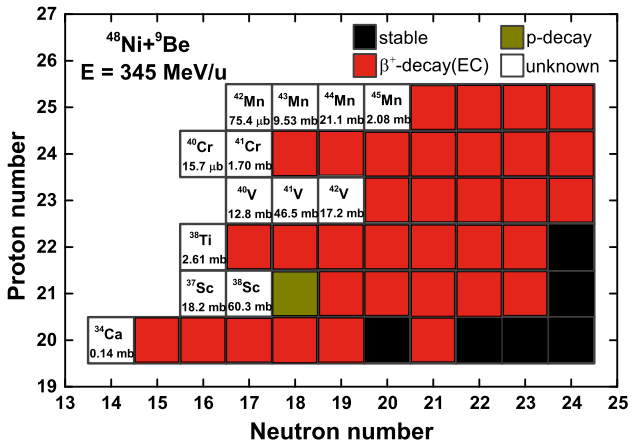

Fig. 5 (Color online) The neutron-deficient nuclei with $Z = 20 - 25$ on the nuclear map. The filled and open squares denote known and unknown nuclei, respectively. Black, red, and brown are stable, β^+ decay, and p decay, respectively. The production cross sections of unknown nuclei in the ^{48}Ni+^{9}Be reaction at 345 MeV/u are indicated by the open squares in the figure

4 Summary

In conclusion, fragmentation isotopic distributions were calculated for ^{58}Ni on ^{9}Be target using the IBLE model for hard and soft symmetry energies. The IBLE model for soft symmetry energy leads to a good description of the cross-section distributions, and the measured cross sections of fragments are reasonably reproduced by the IBLE model, which indicates that the IBLE model can be applied to predict the production cross sections of proton-rich fragments in projectile fragmentation. When considering isospin effects, the ^{48}Ni-induced reaction produces more new nuclei and has the largest production cross sections when compared to the ^{49}Ni and ^{50}Ni projectiles because it has the largest absolute value of isospin and can produce fragments with the greatest proton abundance. Therefore, the ^{48}Ni+^{9}Be reaction is promising for producing proton-rich nuclei with $Z = 20 - 25$. The production cross sections of the new nuclei become larger as the incident energy increases, but this effect becomes weak when the incident energy is higher than 200 MeV/u. The results show that when compared to 140 and 240 MeV/u, the predicted cross sections of new proton-rich nuclei with $Z = 20 - 25$ are the highest at 345 MeV/u. The isospin of the projectile and incident energy play important roles in projectile fragmentations. In the reaction of ^{48}Ni+^{9}Be at 345 MeV/u, 13 new nuclei near the proton drip line were produced in simulations in the vicinity of the projectile ($Z = 28$). The predicted production cross sections of the new nuclei ^{34}Ca, ^{37,38}Sc, ^{38}Ti, ^{40,41,42}V, ^{40,41}Cr, and ^{42,43,44,45}Mn range from 10^{-2} to 10^{2} mb. Hence, the generation of new proton-rich nuclei with $Z = 20 - 25$ via projectile fragmentations using secondary radioactive ion beams of ^{48,49,50}Ni is promising for future studies.

References

1. J. Erler, N. Birge, M. Kortelainen et al., The limits of the nuclear landscape. Nature **486**, 509–512 (2012). https://doi.org/10.1038/nature11188
2. O. Fasoula, G. A. Souliotis, Y. K. Kwon et al., Production cross sections and angular distributions of neutron-rich rare isotopes from 15 MeV/nucleon Kr-induced collisions: toward the r-process path (2021). arXiv:2103.10688 [nucl-th]
3. D.Y. Tao, T.K. Dong, S.J. Yun et al., Short-lived radionuclide production cross sections calculated by the Liège intranuclear cascade model. Phys. Rev. C **103**, 044606 (2021). https://doi.org/10.1103/PhysRevC.103.044606
4. M. Mocko, M.B. Tsang, L. Andronenko et al., Projectile fragmentation of ^{40}Ca , ^{48}Ca , ^{58}Ni , and ^{64}Ni at 140 MeV/nucleon. Phys. Rev. C **74**, 054612 (2006). https://doi.org/10.1103/PhysRevC.74.054612
5. Z.J. Wu, L. Guo, Production of proton-rich actinide nuclei in the multinucleon transfer reaction ^{58}Ni+^{232}Th. Sci. China-Phys. Mech. Astron. **63**, 242021 (2020). https://doi.org/10.1007/s11433-019-1484-0
6. Y. Jin, C.Y. Niu, K.W. Brown et al., First observation of the four-proton unbound nucleus ^{18}Mg. Phys. Rev. Lett. **127**, 262502 (2021). https://doi.org/10.1103/PhysRevLett.127.262502
7. M. Thoennessen, Discovery of nuclides project (2021), https://people.nscl.msu.edu/ thoennes/isotopes. Accessed from 31 Dec 2021
8. M. Thoennessen, Exploring new neutron-rich nuclei with the facility for rare isotope beams. Nucl. Data Sheets **118**, 85–90 (2014). https://doi.org/10.1016/j.nds.2014.04.008
9. K. Langanke, M. Wiescher, Nuclear reactions and stellar processes. Rep. Prog. Phys. **64**, 1657–1701 (2001). https://doi.org/10.1088/0034-4885/64/12/202
10. X.F. Li, D.Q. Fang, Y.G. Ma, Determination of the neutron skin thickness from interaction cross section and charge-changing cross section for section for B, C, N, O, F isotopes. Nucl. Sci. Tech. **27**, 71 (2016). https://doi.org/10.1007/s41365-016-0064-z
11. M. Arnould, S. Goriely, Astronuclear physics: a tale of the atomic nuclei in the skies. Prog. Part. Nucl. Phys. **112**, 103766 (2020). https://doi.org/10.1016/j.ppnp.2020.103766
12. C. Li, P.W. Wen, J.J. Li et al., Production of heavy neutron-rich nuclei with radioactive beams in multinucleon transfer reactions. Nucl. Sci. Tech. **28**, 110 (2017). https://doi.org/10.1007/s41365-017-0266-z
13. P. Danielewicz, R. Lacey, W.G. Lynch, Determination of the equation of state of dense matter. Science **298**, 1592–1596 (2002). https://doi.org/10.1126/science.1078070
14. V. Baran, M. Colonna, V. Greco et al., Reaction dynamics with exotic nuclei. Phys. Rep. **410**, 335–466 (2005). https://doi.org/10.1016/j.physrep.2004.12.004
15. D.V. Shetty, S.J. Yennello, G.A. Souliotis, Density dependence of the symmetry energy and the nuclear equation of state: a dynamical and statistical model perspective. Phys. Rev. C **76**, 024606 (2007). https://doi.org/10.1103/PhysRevC.76.024606
16. B.A. Li, L.W. Chen, C.M. Ko, Recent progress and new challenges in isospin physics with heavy-ion reactions. Phys. Rep. **464**, 113–281 (2008). https://doi.org/10.1016/j.physrep.2008.04.005
17. J.M. Lattimer, M. Prakash, Neutron star observations: prognosis for equation of state constraints. Phys. Rep. **442**, 109–165 (2007). https://doi.org/10.1016/j.physrep.2007.02.003
18. H. Yu, D.Q. Fang, Y.G. Ma, Investigation of the symmetry energy of nuclear matter using isospin-dependent quantum molecular dynamics. Nucl. Sci. Tech. **31**, 61 (2020). https://doi.org/10.1007/s41365-020-00766-x
19. M. Thoennessen, *The Discovery of Isotopes* (Springer, Cham, 2016)
20. D.S. Ahn, N. Fukuda, H. Geissel et al., Location of the neutron dripline at Fluorine and Neon. Phys. Rev. Lett. **123**, 212501 (2019). https://doi.org/10.1103/PhysRevLett.123.212501
21. K. Wimmer, P. Doornenbal, W. Korten et al., Discovery of ^{68}Br in secondary reactions of radioactive beams. Phys. Lett. B **795**, 266–270 (2019). https://doi.org/10.1016/j.physletb.2019.06.014
22. H. Suzuki, L. Sinclair, P.A. Söderström et al., Discovery of ^{72}Rb: a nuclear sandbank beyond the proton drip line. Phys. Rev. Lett. **119**, 192503 (2017). https://doi.org/10.1103/PhysRevLett.119.192503
23. K. Riisager, Halos and related structures. Phys. Scr. **T152**, 014001 (2013). https://doi.org/10.1088/0031-8949/2013/t152/014001
24. R. Kanungo, A new view of nuclear shells. Phys. Scr. **T152**, 014002 (2013). https://doi.org/10.1088/0031-8949/2013/t152/014002
25. H. Geissel, P. Armbruster, K. Behr et al., The GSI projectile fragment separator (FRS): a versatile magnetic system for relativistic heavy ions. Nucl. Instrum. Methods B **70**, 286–297 (1992). https://doi.org/10.1016/0168-583X(92)95944-M
26. H. Geissel, K. Beckert, F. Bosch et al., First storage and cooling of secondary heavy-ion beams at relativistic energies. Phys. Rev. Lett. **68**, 3412–3415 (1992). https://doi.org/10.1103/PhysRevLett.68.3412
27. H.L. Ravn, Experiments with intense secondary beams of radioactive ions. Phys. Rep. **54**, 201–259 (1979). https://doi.org/10.1016/0370-1573(79)90045-0
28. S. Galès, Towards the next generation of radioactive ion beam facilities. Nucl. Phys. A **722**, C148–C156 (2003). https://doi.org/10.1016/S0375-9474(03)01351-4
29. T.J.M. Symons, Y.P. Viyogi, G.D. Westfall et al., Observation of new neutron-rich isotopes by fragmentation of 205-MeV/nucleon ^{40}Ar ions. Phys. Rev. Lett. **42**, 40–43 (1979). https://doi.org/10.1103/PhysRevLett.42.40
30. H. Imal, R. Ogul, Theoretical study of isotope production in the peripheral heavy-ion collision ^{136} Xe + Pb at 1 GeV/nucleon. Nucl. Phys. A **1014**, 122261 (2021). https://doi.org/10.1016/j.nuclphysa.2021.122261
31. F.F. Duan, Y.Y. Yang, B.T. Hu et al., Silicon detector array for radioactive beam experiments at HIRFL-RIBLL. Nucl. Sci. Tech. **29**, 165 (2018). https://doi.org/10.1007/s41365-018-0499-5
32. Z.Y. Sun, W.L. Zhan, Z.Y. Guo et al., Separation and identification of isotopes produced from ^{20}Ne+Be reaction by radioactive ion beam line in Lanzhou. Chin. Phys. Lett. **15**, 790–792 (1998). https://doi.org/10.1088/0256-307X/15/11/004
33. S. Lukyanov, M. Mocko, L. Andronenko et al., Projectile fragmentation of radioactive beams of ^{68} Ni , ^{69} Cu , and ^{72} Zn . Phys. Rev. C **80**, 014609 (2009). https://doi.org/10.1103/PhysRevC.80.014609
34. R.J. Charity, T.B. Webb, J.M. Elson et al., Observation of the exotic isotope ^{13}F located four neutrons beyond the proton drip line. Phys. Rev. Lett. **126**, 132501 (2021). https://doi.org/10.1103/PhysRevLett.126.132501
35. T. Sumikama, N. Fukuda, N. Inabe et al., Observation of new neutron-rich isotopes in the vicinity of ^{110}Zr. Phys. Rev. C **103**, 014614 (2021). https://doi.org/10.1103/PhysRevC.103.014614
36. K. Wang, Y.Y. Yang, A.M. Moro et al., Elastic scattering and breakup reactions of the proton drip-line nucleus ^{8} B on ^{208} Pb at 238 MeV. Phys. Rev. C **103**, 024606 (2021). https://doi.org/10.1103/PhysRevC.103.024606

37. G.G. Adamian, N.V. Antonenko, A. Diaz-Torres et al., How to extend the chart of nuclides? Eur. Phys. J. A **56**, 47 (2020). https://doi.org/10.1140/epja/s10050-020-00046-7
38. D.Q. Fang, W.Q. Shen, J. Feng et al., Measurements of total reaction cross sections for exotic nuclei close to the proton dripline at intermediate energies and observation of a proton halo in ^{27}P. Chin. Phys. Lett. **18**, 1033–1036 (2001). https://doi.org/10.1088/0256-307X/18/8/312
39. C.W. Ma, X.B. Wei, X.X. Chen et al., Precise machine learning models for fragment production in projectile fragmentation reactions by Bayesian neural networks. Chin. Phys. C **46**, 074104 (2022). https://doi.org/10.1088/1674-1137/ac5efb
40. H. Geissel, G. Munzenberg, K. Riisager, Secondary exotic nuclear beams. Annu. Rev. Nucl. Part. Sci. **45**, 163–203 (1995). https://doi.org/10.1146/annurev.ns.45.120195.001115
41. Y. Blumenfeld, T. Nilsson, P. Van Duppen, Facilities and methods for radioactive ion beam production. Phys. Scr. **T152**, 014023 (2013). https://doi.org/10.1088/0031-8949/2013/t152/014023
42. A.M. Poskanzer, G. Butler, E. Hyde et al., Observation of the new isotope ^{17}C using a combined time-of-flight particle-identification technique. Phys. Lett. B **27**, 414–416 (1968). https://doi.org/10.1016/0370-2693(68)90222-0
43. A.M. Poskanzer, S.W. Cosper, E.K. Hyde et al., New Isotopes: ^{11} Li , ^{14} B , and ^{15} B . Phys. Rev. Lett. **17**, 1271–1274 (1966). https://doi.org/10.1103/PhysRevLett.17.1271
44. J.C. David, Spallation reactions: a successful interplay between modeling and applications. Eur. Phys. J. A **51**, 68 (2015). https://doi.org/10.1140/epja/i2015-15068-1
45. H. Alvarez-Pol, J. Benlliure, E. Casarejos et al., Production of new neutron-rich isotopes of heavy elements in fragmentation reactions of ^{238}U projectiles at 1*A* GeV. Phys. Rev. C **82**, 041602 (2010). https://doi.org/10.1103/PhysRevC.82.041602
46. N. Vonta, G.A. Souliotis, W. Loveland et al., Neutron-rich rare-isotope production from projectile fission of heavy nuclei near 20 MeV/nucleon beam energy. Phys. Rev. C **94**, 064611 (2016). https://doi.org/10.1103/PhysRevC.94.064611
47. J. Kurcewicz, F. Farinon, H. Geissel et al., Discovery and cross-section measurement of neutron-rich isotopes in the element range from neodymium to platinum with the FRS. Phys. Lett. B **717**, 371–375 (2012). https://doi.org/10.1016/j.physletb.2012.09.021
48. O.B. Tarasov, M. Portillo, A.M. Amthor et al., Production of very neutron-rich nuclei with a ^{76}Ge beam. Phys. Rev. C **80**, 034609 (2009). https://doi.org/10.1103/PhysRevC.80.034609
49. T. Kurtukian-Nieto, J. Benlliure, K.H. Schmidt et al., Production cross sections of heavy neutron-rich nuclei approaching the nucleosynthesis r-process path around $A = 195$. Phys. Rev. C **89**, 024616 (2014). https://doi.org/10.1103/PhysRevC.89.024616
50. Z. Meisel, S. George, S. Ahn et al., Time-of-flight mass measurements of neutron-rich chromium isotopes up to $N = 40$ and implications for the accreted neutron star crust. Phys. Rev. C **93**, 035805 (2016). https://doi.org/10.1103/PhysRevC.93.035805
51. C. Santamaria, C. Louchart, A. Obertelli et al., Extension of the $N = 40$ island of inversion towards $N = 50$: spectroscopy of ^{66} Cr , ^{70,72} Fe . Phys. Rev. Lett. **115**, 192501 (2015). https://doi.org/10.1103/PhysRevLett.115.192501
52. R. Caballero-Folch, C. Domingo-Pardo, J. Agramunt et al., First measurement of several β-delayed neutron emitting isotopes beyond $N = 126$. Phys. Rev. Lett. **117**, 012501 (2016). https://doi.org/10.1103/PhysRevLett.117.012501
53. K. Palli, G.A. Souliotis, T. Depastas et al., Microscopic dynamical description of multinucleon transfer in ^{40}Ar induced peripheral collisions at 15 MeV/nucleon. EPJ Web Conf. **252**, 07002 (2021). https://doi.org/10.1051/epjconf/202125207002
54. A. Papageorgiou, G.A. Souliotis, K. Tshoo et al., Neutron-rich rare isotope production with stable and radioactive beams in the mass range A $\sim$ 40–60 at beam energy around 15 MeV/nucleon. J. Phys. G **45**, 095105 (2018). https://doi.org/10.1088/1361-6471/aad7df
55. G.A. Souliotis, M. Veselsky, G. Chubarian et al., Enhanced production of neutron-rich rare isotopes in peripheral collisions at Fermi energies. Phys. Rev. Lett. **91**, 022701 (2003). https://doi.org/10.1103/PhysRevLett.91.022701
56. G.A. Souliotis, M. Veselsky, G. Chubarian et al., Enhanced production of neutron-rich rare isotopes in the reaction of 25 MeV/nucleon ^{86}Kr on ^{64}Ni. Phys. Lett. B **543**, 163–172 (2002). https://doi.org/10.1016/S0370-2693(02)02459-0
57. R. Ogul, N. Buyukcizmeci, A. Ergun et al., Production of neutron-rich exotic nuclei in projectile fragmentation at Fermi energies. Nucl. Sci. Tech. **28**, 18 (2016). https://doi.org/10.1007/s41365-016-0175-6
58. R. Thies, A. Heinz, T. Adachi et al., Systematic investigation of projectile fragmentation using beams of unstable B and C isotopes. Phys. Rev. C **93**, 054601 (2016). https://doi.org/10.1103/PhysRevC.93.054601
59. G.F. Bertsch, H. Kruse, S.D. Gupta, Boltzmann equation for heavy ion collisions. Phys. Rev. C **29**, 673–675 (1984). https://doi.org/10.1103/PhysRevC.29.673
60. G.F. Bertsch, S. Das Gupta, A guide to microscopic models for intermediate energy heavy ion collisions. Phys. Rep **160**, 189–233 (1988). https://doi.org/10.1016/0370-1573(88)90170-6
61. O. Buss, T. Gaitanos, K. Gallmeister et al., Transport-theoretical description of nuclear reactions. Phys. Rep. **512**, 1–124 (2012). https://doi.org/10.1016/j.physrep.2011.12.001
62. J. Aichelin, 'Quantum molecular dynamics-a dynamical microscopic n-body approach to investigate fragment formation and the nuclear equation of state in heavy ion collisions. Phys. Rep. **202**, 233–360 (1991). https://doi.org/10.1016/0370-1573(91)90094-3
63. G. Tian, R. Wada, Z. Chen et al., Nuclear stopping and light charged particle emission in ^{12}**C** $+^{12}$ **C** at 95 MeV/nucleon. Phys. Rev. C **95**, 044613 (2017). https://doi.org/10.1103/PhysRevC.95.044613
64. J. Su, L. Zhu, C.C. Guo et al., Uniform description of breakup mechanisms in central collision, projectile fragmentation, and proton-induced spallation. Phys. Rev. C **100**, 014602 (2019). https://doi.org/10.1103/PhysRevC.100.014602
65. Z.Q. Feng, Nuclear dynamics and particle production near threshold energies in heavy-ion collisions. Nucl. Sci. Tech. **29**, 40 (2018). https://doi.org/10.1007/s41365-018-0379-z
66. C.W. Ma, C.Y. Qiao, T.T. Ding et al., Temperature of intermediate mass fragments in simulated ^{40}**Ca** $+^{40}$ **Ca** reactions around the Fermi energies by AMD model. Nucl. Sci. Tech. **27**, 111 (2016). https://doi.org/10.1007/s41365-016-0112-8
67. A. Guarnera, M. Colonna, P. Chomaz, 3D stochastic mean-field simulations of the spinodal fragmentation of dilute nuclei. Phys. Lett. B **373**, 267–274 (1996). https://doi.org/10.1016/0370-2693(96)00152-9
68. M. Colonna, M. Di Toro, A. Guarnera et al., Fluctuations and dynamical instabilities in heavy-ion reactions. Nucl. Phys. A **642**, 449–460 (1998). https://doi.org/10.1016/S0375-9474(98)00542-9
69. J.J. Gaimard, K.H. Schmidt, A reexamination of the abrasion-ablation model for the description of the nuclear fragmentation reaction. Nucl. Phys. A **531**, 709–745 (1991). https://doi.org/10.1016/0375-9474(91)90748-U

70. C.W. Ma, H.L. Wei, J.Y. Wang et al., Isospin dependence of projectile-like fragment production at intermediate energies. Phys. Rev. C **79**, 034606 (2009). https://doi.org/10.1103/PhysRevC.79.034606
71. D.Q. Fang, W.Q. Shen, J. Feng et al., Isospin effect of fragmentation reactions induced by intermediate energy heavy ions and its disappearance. Phys. Rev. C **61**, 044610 (2000). https://doi.org/10.1103/PhysRevC.61.044610
72. K. Sümmerer, Erratum: improved empirical parametrization of fragmentation cross sections [Phys. Rev. C 86, 014601 (2012)]. Phys. Rev. C **87**, 039903 (2013). https://doi.org/10.1103/PhysRevC.87.039903
73. K. Sümmerer, Improved empirical parametrization of fragmentation cross sections. Phys. Rev. C **86**, 014601 (2012). https://doi.org/10.1103/PhysRevC.86.014601
74. K. Sümmerer, B. Blank, Modified empirical parametrization of fragmentation cross sections. Phys. Rev. C **61**, 034607 (2000). https://doi.org/10.1103/PhysRevC.61.034607
75. G. Rudstam, Systematics of spallation yields. Z. Naturforsch. Teil A **21**, 1027–1041 (1966). https://doi.org/10.1515/zna-1966-0724
76. B. Mei, Improved empirical parameterization for projectile fragmentation cross sections. Phys. Rev. C **95**, 034608 (2017). https://doi.org/10.1103/PhysRevC.95.034608
77. Y.D. Song, H.L. Wei, C.W. Ma et al., Improved fracs parameterizations for cross sections of isotopes near the proton drip line in projectile fragmentation reactions. Nucl. Sci. Tech. **29**, 96 (2018). https://doi.org/10.1007/s41365-018-0439-4
78. H. Wolter, M. Colonna, D. Cozma et al., Transport model comparison studies of intermediate-energy heavy-ion collisions (2022). arXiv: 2202.06672 [nucl-th]
79. C.W. Ma, Y.L. Zhang, S.S. Wang et al., A model comparison study of fragment production in 140 *A* MeV ^{58,64}Ni+^{9}Be reactions. Chin. Phys. Lett. **32**, 072501 (2015). https://doi.org/10.1088/0256-307X/32/7/072501
80. Y.X. Zhang, N. Wang, Q.F. Li et al., Progress of quantum molecular dynamics model and its applications in heavy ion collisions. Front. Phys. **15**, 54301 (2020). https://doi.org/10.1007/s11467-020-0961-9
81. M. Colonna, Collision dynamics at medium and relativistic energies. Prog. Part. Nucl. Phys. **113**, 103775 (2020). https://doi.org/10.1016/j.ppnp.2020.103775
82. J. Xu, Transport approaches for the description of intermediate-energy heavy-ion collisions. Prog. Part. Nucl. Phys. **106**, 312–359 (2019). https://doi.org/10.1016/j.ppnp.2019.02.009
83. A. Ono, Dynamics of clusters and fragments in heavy-ion collisions. Prog. Part. Nucl. Phys. **105**, 139–179 (2019). https://doi.org/10.1016/j.ppnp.2018.11.001
84. C.W. Ma, Y.G. Ma, Shannon information entropy in heavy-ion collisions. Prog. Part. Nucl. Phys. **99**, 120–158 (2018). https://doi.org/10.1016/j.ppnp.2018.01.002
85. C.W. Ma, H.L. Wei, X.Q. Liu et al., Nuclear fragments in projectile fragmentation reactions. Prog. Part. Nucl. Phys. **121**, 103911 (2021). https://doi.org/10.1016/j.ppnp.2021.103911
86. Y. Abe, S. Ayik, P.G. Reinhard et al., On stochastic approaches of nuclear dynamics. Phys. Rep. **275**, 49–196 (1996). https://doi.org/10.1016/0370-1573(96)00003-8
87. F.S. Zhang, E. Suraud, Boltzmann-Langevin equation, dynamical instability and multifragmentation. Phys. Lett. B **319**, 35–40 (1993). https://doi.org/10.1016/0370-2693(93)90777-F
88. F.S. Zhang, E. Suraud, Analysis of multifragmentation in a Boltzmann-Langevin approach. Phys. Rev. C **51**, 3201 (1995). https://doi.org/10.1103/PhysRevC.51.3201
89. S. Ayik, C. Grégoire, Fluctuations of single-particle density in nuclear collisions. Phys. Lett. B **212**, 269–272 (1988). https://doi.org/10.1016/0370-2693(88)91315-9
90. W. Bauer, G.F. Bertsch, S. Das Gupta, Fluctuations and clustering in heavy-ion collisions. Phys. Rev. Lett **58**, 863–866 (1987). https://doi.org/10.1103/PhysRevLett.58.863
91. P. Chomaz, G. Burgio, J. Randrup, Inclusion of fluctuations in nuclear dynamics. Phys. Lett. B **254**, 340–346 (1991). https://doi.org/10.1016/0370-2693(91)91166-S
92. E. Suraud, S. Ayik, M. Belkacem et al., Applications of Boltzmann-Langevin equation to nuclear collisions. Nucl. Phys. A **542**, 141–158 (1992). https://doi.org/10.1016/0375-9474(92)90403-7
93. J. Randrup, B. Remaud, Fluctuations in one-body dynamics. Nucl. Phys. A **514**, 339–366 (1990). https://doi.org/10.1016/0375-9474(90)90075-W
94. W.J. Xie, J. Su, L. Zhu et al., Symmetry energy and pion production in the Boltzmann-Langevin approach. Phys. Lett. B **718**, 1510–1514 (2013). https://doi.org/10.1016/j.physletb.2012.12.021
95. B. Li, N. Tang, F.S. Zhang, Isospin effects of projectile fragmentation in a Boltzmann-Langevin approach. Chin. Phys. C **45**, 084103 (2021). https://doi.org/10.1088/1674-1137/ac009a
96. B.A. Bian, F.S. Zhang, H.Y. Zhou, Fragmentation cross sections of ^{20}Ne collisions with different targets at 600 MeV/nucleon. Nucl. Phys. A **807**, 71–78 (2008). https://doi.org/10.1016/j.nuclphysa.2008.03.014
97. K. Chen, Z. Fraenkel, G. Friedlander et al., VEGAS: a monte carlo simulation of intranuclear cascades. Phys. Rev. **166**, 949–967 (1968). https://doi.org/10.1103/PhysRev.166.949
98. S. Huber, J. Aichelin, Production of Δ- and N*-resonances in the one-boson exchange model. Nucl. Phys. A **573**, 587–625 (1994). https://doi.org/10.1016/0375-9474(94)90232-1
99. J. Cugnon, D. L'Hôte, J. Vandermeulen, Simple parametrization of cross-sections for nuclear transport studies up to the GeV range. Nucl. Instrum. Meth. B **111**, 215–220 (1996). https://doi.org/10.1016/0168-583X(95)01384-9
100. Y.D. Song, H.L. Wei, C.W. Ma, Fragmentation binding energies and cross sections of isotopes near the proton dripline. Phys. Rev. C **98**, 024620 (2018). https://doi.org/10.1103/PhysRevC.98.024620
101. C.W. Ma, Y.D. Song, H.L. Wei, Binding energies of near proton-drip line Z = 22–28 isotopes determined from measured isotopic cross section distributions. Sci. China-Phys. Mech. Astron. **62**, 012013 (2019). https://doi.org/10.1007/s11433-018-9256-8